Density Functional Theory Investigations of the Direct Oxidation of Methane on an Fe-Exchanged Zeolite

WanZhen Liang,[†,‡,§] Alexis T. Bell,*[,†] Martin Head-Gordon,[‡] and Arup K. Chakraborty[†,‡]

Department of Chemical Engineering and Department of Chemistry, University of California, Berkeley, California 94720

Received: July 30, 2003; In Final Form: November 7, 2003

The reactions of methane with $[FeO_2]^+$ and $[OFeO)]^+$ cations exchanged into ZSM-5 have been investigated using density functional theory. Experimental evidence for the latter cation has recently been reported on the basis of EXAFS experiments performed on Fe−ZSM-5 with Fe/Al = 0.17−0.80. Of the two iron-containing species investigated, Z[OFeO] [Z here represents the cation-exchange site in the zeolite] is lower in energy by 7.7 kcal/mol, assuming a spin multiplicity $M = 6$. The activation energy for the conversion of $Z[FeO_2]$ and Z[OFeO] is 10.0 kcal/mol. The activation of methane occurs preferentially on Z[OFeO]. Weakly adsorbed methane reacts with Z[OFeO] to produce a weakly bound $CH_3^{\bullet}$ free radical. The activation barrier for this process is 15.9 kcal/mol. The methyl radical then reacts via a barrierless process to form $Z[(OH)Fe(OCH_3)]$. This product is very stable thermally, but can be converted to adsorbed methanol or formaldehyde via processes exhibiting high activation barriers (∼39.3 kcal/mol in both cases). Hydrolysis of $Z[(OH)Fe(OCH_3)]$ to form adsorbed methanol is practically thermoneutral and has an activation barrier of 6.2 kcal/mol. The desorption of the adsorbed methanol is endothermic by 18.8 kal/mol, but the formation of water from the resulting $Z[Fe(OH)_2]$ has a moderately high activation barrier of 37.9 kcal/mol. If N_2O is present in the gas phase, the activation barrier for the formation of H_2O decreases to 18.1 kcal/mol. The results of the present investigation are qualitatively consistent with recent experimental observations.

Introduction

Several studies have shown that an Fe-exchanged ZSM-5 zeolite pretreated at an elevated temperature with N_2O and then exposed to methane at room temperature will produce methoxide species.[1,2] Methanol can then be produced by the reaction of these species with water vapor at room temperature. Methoxide species bound to Fe have also recently been observed when a mixture of N_2O and CH_4 is contacted with Fe−ZSM-5 at temperatures above 523 K.[3] These observations have stimulated an interest in defining the nature of the iron and oxygen species involved in the formation of methoxide groups and the energetics for the conversion of these groups to either methanol or fomaldehyde. Experimental evidence from EXAFS and Mössbauer has been put forward for both mono iron and diron oxo species [e.g., Z[FeO], $Z[Fe(O)_2]$, and $Z[(OH)Fe(OH)_2Fe(OH)]$.[4−14] Although the oxygen species involved in the activation of methane have not been identified experimentally, $[Fe{=}O]^+$ and $[Fe(O)_2Fe]^+$ species have been proposed as the catalytically active centers on the basis of quantum chemical calculations.[15−17]

We have recently reported a quantum chemical analysis of the pathway for N_2O decomposition over Fe−ZSM-5. This work suggests that $[Fe(O)_2]^+$ is a key intermediate along the reaction pathway and is the most abundant species during steady-state N_2O decomposition.[18] The calculated apparent activation energy is very close to that observed experimentally.[12] In a subsequent theoretical study, we showed that $[Fe(O)_2]^+$ cations could also be responsible for the oxidation of benzene to phenol.[19] The validity of this proposal was supported by the close agreement of the calculated apparent activation energy and the turnover frequency for phenol formation with values of the corresponding quantities measured experimentally. Evidence for the presence of $[Fe(O)_2]^+$ cations in Fe−ZSM-5 is further supported by EXAFS studies we have performed, which suggest that at Fe/Al ratios of 0.17−0.80 all of the Fe is present as $[Fe(O)_2]^+$ or $[Fe(OH)_2]^+$.[20] The objective of the present investigation was to investigate whether mono-iron di-oxygen species would react with methane to form methoxide and hydroxide species, i.e., $[Fe(OCH_3)(OH)]^+$. The thermal stability of such species and their reactivity with water vapor were also examined. All of the work was carried out using density functional theory (DFT).

Theoretical Methods

The structure and properties of mono-iron di-oxygen species located at cations-exchange sites in a zeolite were investigated using density functional theory (DFT). The zeolite was represented by a cluster consisting of an Al atom coupled through O atoms to two Si atoms. The cluster was terminated by two OH groups attached to the Al atom and three H atoms attached to each of the Si atoms. Three configurations of the O and Fe atoms were considered based on previous quantum chemical studies showing that neutral FeO_2 and cationic FeO_2^+ are stable as FeOO ($FeOO^+$), a superoxo species; OFeO ($OFeO^+$), a dioxo species; and $Fe(O_2)$ ($Fe(O_2)^+$), a peroxo species.[21−23]

Prior studies have shown that the assignment of the ground state for mono-iron di-oxygen species is strongly dependent on the level of theory. Whereas DFT is considered to be one of the most reliable methods for studying such structures, the configuration of the ground state is found to depend on the form of the exchange-correlation function used and the size of the basis set. Since there is no theoretical basis for selecting the best combination of exchange−correlation functional and basis set, the choice must be made empirically. In practice, this requires the selection of the exchange−correlation functional

* To whom correspondence should be addressed. E-mail: alexbell@uclink.berkeley.edu.
† Department of Chemical Engineering.
‡ Department of Chemistry.
§ Present address: Laboratory of Bond Selective Chemistry, University of Science and Technology of China, Hefei 230026, P. R. China.

10.1021/jp030929g CCC: $27.50
Published on Web 03/12/2004

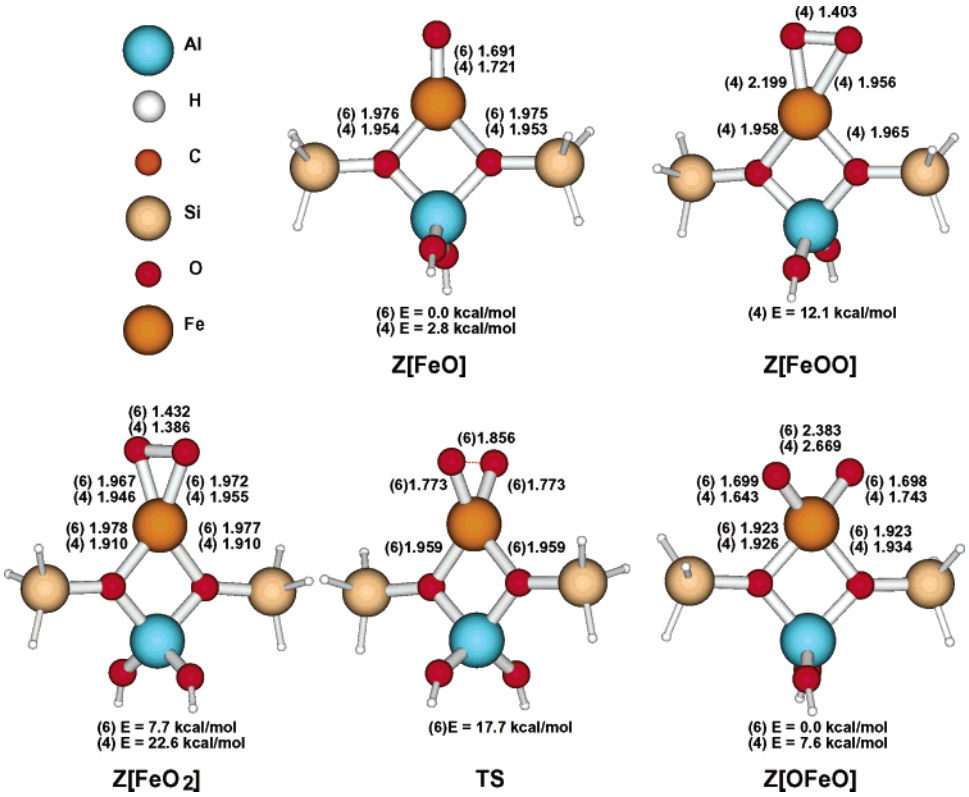

Figure 1. Energies and geometries of Z[FeO], Z[FeOO], Z[FeO_2], and Z[OFeO]. The spin multiplicity of each species is shown in paretheses.

TABLE 1: Energies, Spin Multiplicities, and Geometries of OFeO

		energy (Hartree)		R_{FeO} (Å)		∠ OFeO (°)	
method	basis set	$M = 3$	$M = 5$	$M = 3$	$M = 5$	$M = 3$	$M = 5$
B3LYP	6-31G**	−1413.9575	−1413.9637	1.574	1.592	144.270	118.532
B3LYP	CRENBL	−155.3260	−155.2998	1.598	1.675	138.088	98.667
B3LYP	LANL2DZ	−273.7439	−273.7473	1.620	1.639	148.884	115.792
B3LYP	SRSC	−274.3024	−273.3088	1.619	1.700	147.116	117.936
B3PW91	6-31G**	−14113.8374	−1413.8448	1.567	1.585	143.507	118.329
B3PW91	CRENBL	−155.3604	−155.3306	1.588	1.666	148.359	115.752
B3PW91	LANL2DZ	−273.6966	−273.7010	1.613	1.633	148.359	115.752
B3PW91	SRSC	−274.2478	−274.2552	1.609	1.622	146.340	117.652

and basis set combination that leads to a ground-state multiplicity, Fe−O bond distances and O−Fe−O angles, and Fe−O vibrational frequencies that are consistent with those measured for the experimentally observed dioxo, OFeO structure.[21] For the present study, we considered both the nonlocal, gradient-corrected density functionals B3PW91[24] and B3LYP[25] and the split valence basis set 6-31G**, effective core potential basis CRENBL,[26] LANL2DZ,[27] and SRSC.[28] As shown in Table 1, the calculated O−Fe−O bond angles for the triplet state determined using the B3LYP and B3PW91 density functionals together with the effective core potential basis sets listed above are consistent with that determined experimentally, 144 ± 5°.[21] By contrast, the calculated O−FeO bond angles for the quintet state are far from the experimental value. Based on this observation, the spin multiplicity of OFeO in the ground state should be a triplet. However, only the B3LYP/CRENBL and B3PW91/CRENBL combinations result in the prediction that the total energy of the triplet ground state is lower than that of the quintet state. The calculated Fe−O vibrational frequencies, 1024.1 and 770.3 cm^{-1} determined using B3LYP/CRENBL and 1027.2 and 682.6 cm^{-1} determined using B3PW91/CRENBL, are also consistent with those observed, 945.8 and 797.1 cm^{-1}.[21] Since the B3LYP/CRENBL combination gave better overall consistency with experiments, we used this combination for all of the work reported here. The effects of adding polarization functions on single-point energies were also explored. Calculations were performed for three isomers—Z[FeO_2], Z[OFeO], and Z[FeOO]—assuming spin multiplicities of $M = 2$, 4, and 6. The geometry of each structure was fully optimized using the gradient techniques within the Q-Chem package.[29]

Results and Discussion

Based on calculations done with the B3LYP/CRENBL, the ground states of Z[OFeO] and Z[FeO_2] were identified as sextets, and the ground state of Z[FeOO] was identified as a quartet state. The lowest energy isomer is Z[OFeO] ($M = 6$), whereas the energies of Z[FeO_2] ($M = 6$) and Z[FeOO] ($M = 4$) lie 7.7 and 12.1 kcal/mol higher than that of Z[OFeO]. The observation of Z[OFeO] as the lowest energy state is consistent with studies of gas-phase iron-dioxygen adducts, which show that the formal iron(V) compound $(FeO_2)^+$ can easily interconvert into the lower energy $(OFeO)^+$.[29] The geometries of the three iron dioxo species are shown in Figure 1. Z[FeO_2] is a side-on peroxo complex in which the Fe−O bond length is 1.96 Å. This is longer than the Fe−O bond length of 1.69 Å in OFeO. As a consequence, O_2 is weakly bonded to iron in Z[FeO_2]. Molecular oxygen O_2 is a paramagnetic molecule, having a triplet $^3\Sigma_g$ ground state. The addition of one or two electrons to a neutral dioxygen molecule results in formation of the

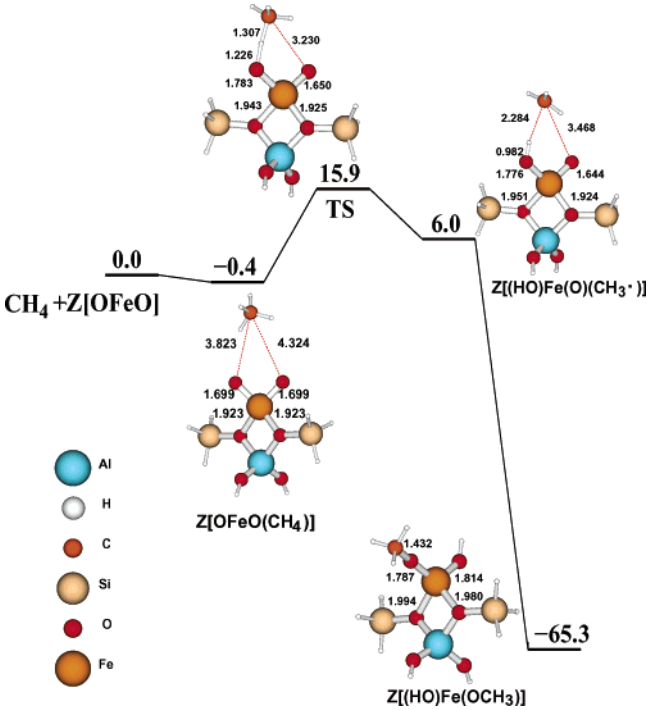

Figure 2. Reaction-energy diagram for the interaction of CH_4 with Z[OFeO] ($M = 6$) to form Z[(HO)Fe(OCH_3)] via a free-radical pathway (see text).

superoxide O_2^- and peroxide O_2^{-2} anions, respectively. The bond order of the O_2^- is larger than that of O_2^{-2}, and correspondingly, the O−O bond length of O_2^- is shorter than that of the O_2^{2-}.[30] Based on these observations, the di-oxygen species in Z[FeOO], for which the O−O bond length is 1.403 Å, is best described as a superoxide, whereas the oxygen species in Z[FeO_2], for which the O−O bond length is 1.432 Å, is best described as a peroxide. These assignments parallel those made for gas-phase FeO_2^+ cations.[21] For Z[OFeO], the O−O bond distance is 2.383 Å, indicating the complete absence of a O−O bond. As noted in Figure 1, the transition state for the conversion of Z[FeO_2] ($M = 6$) to Z[OFeO] ($M = 6$) is 10. 0 kcal/mol.

The interactions of Z[OFeO] and Z[FeO_2] with CH_4 were examined separately. In each case, the CRENBL basis set was used. The effects of adding polarization functions to this basis set are discussed in the Appendix. Z[OFeO] reacts via a weakly bound free methyl radical to form Z[$HOFeOCH_3$] as shown below:

$$Z[OFeO] + CH_4 \rightarrow Z[OFeO(CH_4)] \quad (1)$$

$$Z[OFeO(CH_4)] \rightarrow Z[(HO)FeO(CH_3^{\bullet})] \quad (2)$$

$$Z[(HO)FeO(CH_3^{\bullet})] \rightarrow Z[(HO)Fe(OCH_3)] \quad (3)$$

As seen in Figure 2, the reaction begins with the adsorption of CH_4. The binding energy for this process is only −0.4 kcal/mol. Adsorbed CH_4 then reacts with one of the oxygen atoms bound to Fe to form a hydroxyl group and a weakly bound methyl radical. This reaction is endothermic by 6.4 kcal/mol and has an activation barrier of 15.9 kcal/mol. As the reaction proceeds, the Fe−O bond length for the O atom that reacts with an H atom of CH_4 increases in length from 1.699 to 1.783 Å, whereas the other Fe−O bond length decreases from about 1.699 to 1.650 Å. The intermediate Z[(HO)FeO($CH_3^{\bullet}$)] is similar in character to that proposed in biological systems.[31] This state is apparently not stable. A transition state for its conversion to Z[(HO)Fe(OCH_3)] cannot be found, and even minor perturbations in the structure of Z[(HO)FeO($CH_3^{\bullet}$)] result in the stabilization of Z[(HO)Fe(OCH_3)]. As a consequence, reaction 3 is assumed to be barrierless. The exothermicity of this reaction is −71.3 kcal/mol, whereas the overall energy change for reactions 1−3 is −65.3 kcal/mol.

Figure 3 illustrates the possible pathways by which Z[(HO)-Fe(OCH_3)] can react to form adsorbed CH_3OH or CH_2O. These reactions can be written as

$$Z[(HO)Fe(OCH_3)] \rightarrow Z[OFe(HOCH_3)] \quad (4)$$

$$Z[(HO)Fe(OCH_3)] \rightarrow Z[(H_2O)Fe(OCH_2)] \quad (5)$$

$$Z[(HO)Fe(OCH_3)] \rightarrow Z[OFe(OCH_2)(H_2)] \quad (6)$$

The changes in all bond distances are also shown in Figure 3. Reactions 4 and 5 have virtually identical activation energies of ∼39.3 kcal/mol, and both are endothermic, the first by 24.8 kcal/mol and the second by 34.2 kcal/mol. Reaction 6 is similar to reaction 5 but results in desorption of H_2. The activation energy for reaction 6 is 70.6 kcal/mol and its endothermicity is 62.6 kcal/mol. The theoretical predictions presented in Figure 3 are consistent with recent experimental observations.[3] Studies of the thermal stability of methoxide species on Fe−ZSM-5 have shown that the methoxide species disappear rapidly at temperatures above 623 K ($\tau \sim 10-20$ s). Assuming a preexponential factor of 10^{13} s^{-1}, this decomposition temperature is fully consistent with the calculated activation barrier of 39 kcal/mol ($\tau = 5$ s).

The reaction of Z[(HO)Fe(OCH_3)] with H_2O to form CH_3-OH proceeds via three steps:

$$Z[(HO)Fe(OCH_3)] + H_2O \rightarrow Z[(HO)Fe(OCH_3)(H_2O)] \quad (7)$$

$$Z[(HO)Fe(OCH_3)(H_2O)] \rightarrow Z[Fe(OH)_2(CH_3OH)] \quad (8)$$

$$Z[Fe(OH)_2(CH_3OH)] \rightarrow Z[Fe(OH)_2] + CH_3OH \quad (9)$$

Figure 4 shows that the adsorption of H_2O, reaction 7, is exothermic by −17.3 kcal/mol, whereas the hydrolysis of the Fe−O bond in the methoxide species, reaction 8, is virtually thermoneutral and has an activation barrier of 6.2 kcal/mol. Desorption of CH_3OH, reaction 9, is endothermic by 18.8 kcal/mol. These results are fully consistent with experimental observations, which show that Fe−OCH_3 is readily converted to methanol by reaction with water vapor at room temperature.[2,3] To restore the catalyst to its initial state, the two hydroxyl groups associated with the iron center must first react to form water. This reaction and the subsequent desorption of H_2O can be written as

$$Z[Fe(OH)_2] \rightarrow Z[FeO(H_2O)] \quad (10)$$

$$Z[FeO(H_2O)] \rightarrow Z[FeO] + H_2O \quad (11)$$

According to Figure 4, the first of these reactions has an activation energy of 37.9 kcal/mol and is endothermic by 15.8 kcal/mol. Desorption of water via reaction 11 requires 40.8 kcal/mol. Thus, although it is very easy to form adsorbed methanol by the reaction of water with Z[$HOFeOCH_3$], the desorption of CH_3OH is mildly endothermic and the condensation of hydroxyl groups and the subsequent desorption of H_2O is highly endothermic. The initial state of the active site is achieved via the

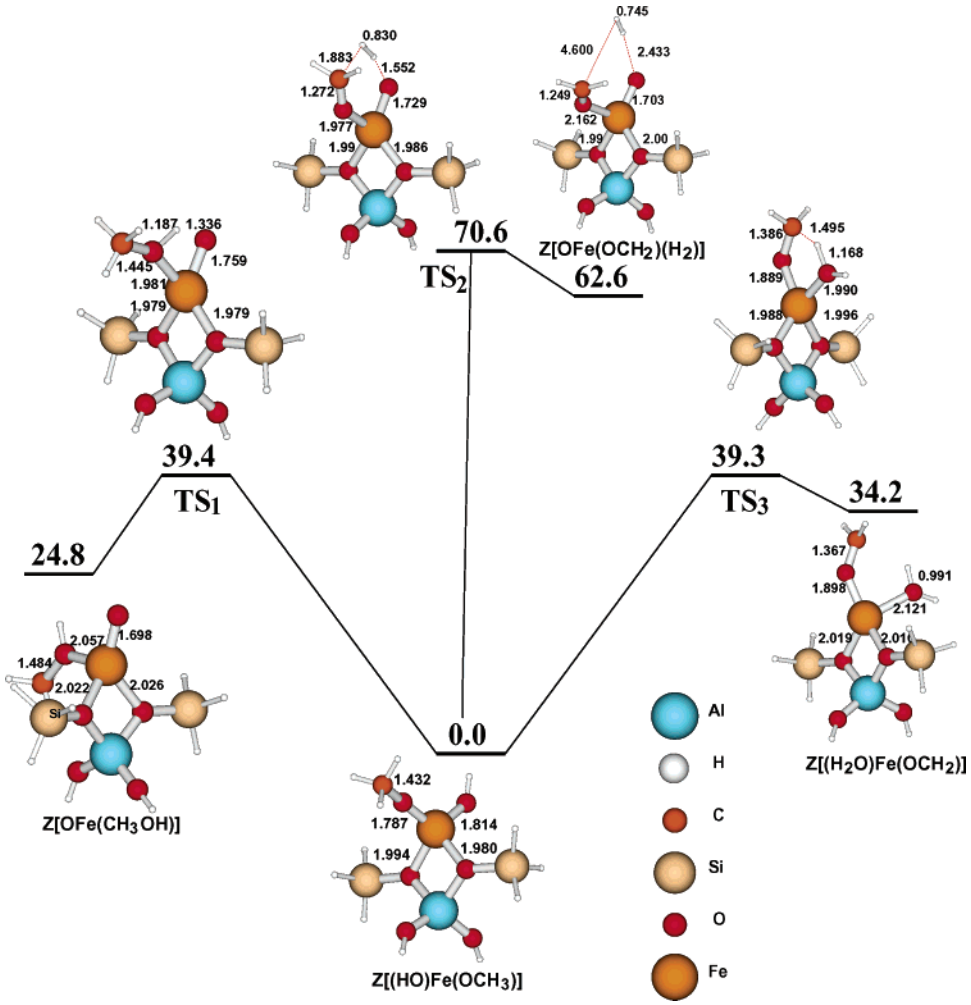

Figure 3. Reaction-energy diagram for the rearrangement of Z[(HO)Fe(OCH_3)] to form Z[OFe(CH_3OH)], Z[OFe(OCH_2)(H_2)], and Z[(H_2O)Fe(OCH_2)].

reaction of Z[FeO] with N_2O − Z[FeO] + N_2O → Z[OFeO] + N_2, a process that is exothermic by −21.9 kcal/mol.

Given the high activation barrier for reaction 10, an alternative path to the release of water was examined. In the first step, Z[Fe($OH)_2$] reacts with N_2O to form Z[Fe(O)($OH)_2$] and N_2. This process is endothermic by 18.0 kcal/mol. Z[Fe(O)($OH)_2$] then rearranges to produce Z[OFeO(H_2O)]. The activation barrier for this process is 18.1 kcal/mol and the reaction is exothermic by −17.2 kcal/mol. The desorption of H_2O from Z[OFeO(H_2O)] is endothermic by 33.8 kcal/mol. However, even though this value is lower than that for the desorption of H_2O from Z[FeO(H_2O)], 40.8 kcal/mol, the desorption of water is projected to remain as a difficult step in the regeneration of the active site.

In the case of Z[FeO_2], the reaction with CH_4 leads to a methoxide group via a bound methyl group, which is formed through a concerted process

$$Z[FeO_2] + CH_4 \rightarrow Z[FeO_2(CH_4)] \quad (12)$$

$$Z[FeO_2(CH_4)] \rightarrow Z[(HOO)Fe(CH_3)] \quad (13)$$

$$Z[(HOO)Fe(CH_3)] \rightarrow Z[OFe(OH)(CH_3)] \quad (14)$$

$$Z[OFe(OH)(CH_3)] \rightarrow Z[(HO)Fe(OCH_3)] \quad (15)$$

Figure 5 demonstrates that the energetics of reactions 12−15 depend on the spin states of molecules. The reaction pathway for Fe in the sextet state is shown as a solid line, and that for the quartet state, as a dashed line. Reaction 13 begins with the cleavage of a C−H bond in CH_4 to form a hydroperoxyl and a methyl group. This step is endothermic by 9.1 kcal/mol for $M = 6$ and 13.1 kcal for $M = 4$. Correspondingly, the activation barriers are 36.9 and 49.8 kcal/mol. The hydroperoxyl group then dissociates into oxo and hydroxyl groups, a step that is exothermic by −9.6 kcal/mol for $M = 6$ and −34.8 for $M = 4$ and the corresponding activation energies are 14.2 and 8.4 kcal/mol. Z[(HO)Fe(OCH_3)] is then formed by the migration of the methyl group in Z[OFe(OH)(CH_3)] to the oxo group. This step is exothermic by −71.5 kcal/mol for $M = 6$ and by −35.9 kcal/mol for $M = 4$. The activation barrier from the quartet state is 8.1 kcal/mol. Since a transition state could not be found for the same process proceeding through the sextet state, the barrier for this pathway is not known.

It is evident from Figure 5 that there are at least two places along the reaction pathway where the quartet and sextet potential energy surfaces can cross. Because of the large spin−orbit coupling of Fe, spin inversion, a nonadiabatic process, could occur. A similar finding has been reported previously for the conversion of methane to methanol by Z[FeO][16] and for the gas-phase reaction of methane with $(FeO)^+$ to form methanol.[32−35] In the latter case, Shaik et al.[36] have proposed that the phenomenon of "two state" reactivity should occur in reactions catalyzed by organometallic complexes, in contrast to organic reactions for which one state plays a dominant role.

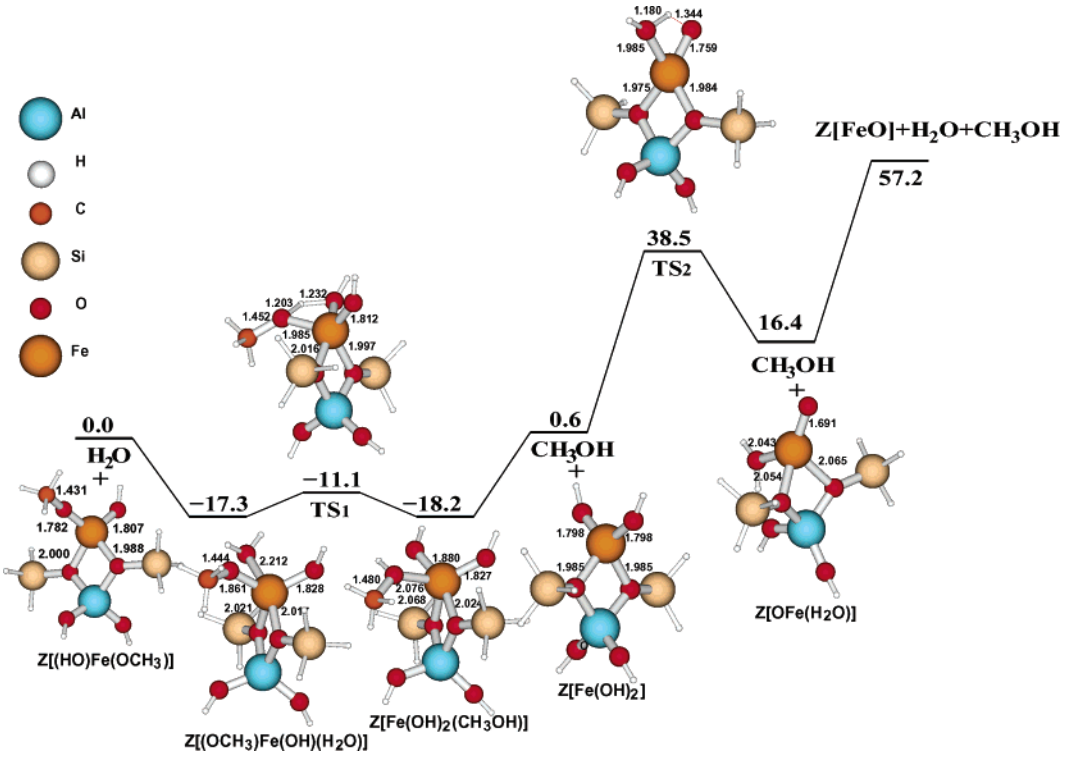

Figure 4. Reaction-energy diagram for the hydrolysis of Z[(HO)Fe(OCH_3)] to form CH_3OH and Z[Fe$(OH)_2$] and for the dehydration of Z[Fe$(OH)_2$] to form H_2O and Z[Fe$(OH)_2$].

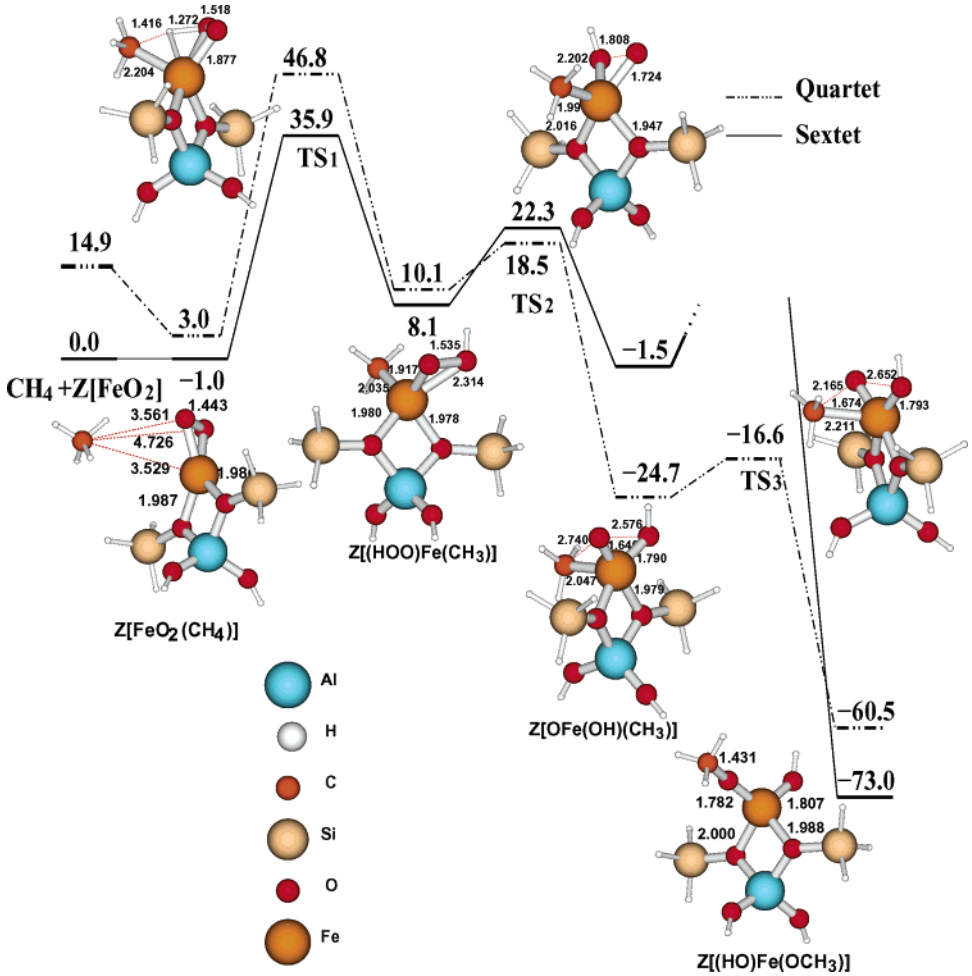

Figure 5. Reaction-energy diagram for the interaction of CH_4 with Z[FeO_2] to form Z[(HO)Fe(OCH_3)] via a concerted pathway at different spin multiplicities $M = 4$ and 6, respectively. The geometry on each stationary point is corresponding to the lower energy state.

TABLE 2: Relative Energies (in kcal/mol) of All Stationary Points Shown in Figures 2−5 with and without the Use of Polarization Functions[a]

structure	Figure	E_{rel}(CRENBL)		E_{rel}(CRENBL+pol)	
CH_4+Z(OFeO)	2	0.0		0.0	
Z[OFeOCH_4)]	2	−0.4		−0.3	
TS	2	15.9		13.6	
Z[(HO)Fe(O)($CH_3^{\bullet}$)]	2	6.0		0.2	
Z[(HO)Fe(OCH_3)]	2	−65.3		−74.5	
Z[OFe(CH_3OH)]	3	24.8		25.4	
TS_1	3	39.4		39.6	
Z[(HO)Fe(OCH_3)]	3	0.0		0.0	
TS_2	3	70.6		66.2	
Z[OFe(OCH_2)(H_2)]	3	62.6		56.4	
TS_3	3	39.3		35.9	
Z[(H_2O)]Fe(OCH_2)]	3	34.2		27.3	
H_2O+Z[(HO)Fe(OCH_3)]	4	0.0		0.0	
Z[(OCH_3)Fe(OH)(H_2O)]	4	−17.3		−14.6	
TS_1	4	−11.1		−4.5	
Z[Fe$(OH)_2$(CH_3OH)]	4	−18.2		−13.1	
CH_3OH+Fe$(OH)_2$	4	0.6		1.3	
TS_2	4	38.5		40.8	
CH_3OH+Z[OFe(H_2O)]	4	16.4		20.8	
CH_3OH+H_2O+Z[FeO]	4	57.2		52.8	
CH_4+Z[Fe(O_2)]	5	14.9	0.0	9.8	0.0
Z[Fe(O_2)(CH_4)]	5	−3.0	−1.0	2.0	−0.6
TS_1	5	46.8	35.9	43.7	37.1
Z[(HOO)Fe(CH_3)]	5	10.1	8.1	7.8	7.3
TS_2	5	18.5	22.3	19.8	25.2
Z[OFe(OH)(CH_3)]	5	−24.7	−1.5	−21.7	2.3
TS_3	5	−16.6		−14.4	
Z[(HO)Fe(OCH_3)]	5	−60.5	−73.0	−59.1	−72.7

[a] All calculations used the CRENBL optimized geometries shown in Figures 2−5 and the B3LYP functional. Two sets of values for Figure 5 correspond to quartet states (first column) and sextet states (second column).

Comparison of the reaction pathways to methane to Z[Fe(HO)(OCH_3)] via Z[OFeO] and Z[FeO_2] (see Figures 2 and 5) strongly suggests that reaction involving the first of these species will be favored because of the significantly smaller reaction barrier [15.9 versus 36.9 kcal/mol (see Figure 5)] required for the first step. The facile conversion of Z[FeO_2] to Z[OFeO] should also contribute to the occurrence of the reaction of methane via the latter species.

Conclusions

The reaction of methane with di-oxygen species in Fe exchanged into a zeolite has been examined by means of quantum chemical calculations. Two principal species have been identified, for the activation of CH_4. The first is the di-oxo species Z[OFeO] and the second is the peroxo species Z[FeO_2]. The ground state of Z[FeO_2] lies 7.7 kcal/mol higher than that of Z[OFeO]. The activation energy for the conversion of Z[FeO_2] ($M = 6$) to Z[OFeO] ($M = 6$) is 10.0 kcal/mol. The activation of methane and subsequent formation of iron methoxide species occurs preferentially via Z[OFeO]. Weakly adsorbed CH_4 first produces a $CH_3^{\bullet}$ radical, which then reacts via a barrier-less process to form Z[(HO)Fe(OCH_3)]. The latter species is very stable but can undergo reactions with high activation barriers to form adsorbed methanol or formaldehyde. The hydrolysis of Z[(HO)Fe(OCH_3)] to form adsorbed methanol occurs with only a small activation barrier and is thermoneutral. Whereas the desorption of the adsorbed methanol has an activation barrier of only 18.8 kcal/mol, the release of water from the byproduct, Z[Fe$(OH)_2$], has an activation barrier of 37.9 kcal/mol. If N_2O is present in the gas phase, the release of water could proceed via an alternate pathway for which the activation barrier is 18.1 kcal/mol. Thus, the results of this study show that the formation of iron methoxide species via the reaction of CH_4 with iron di-oxo species present in a zeolite is a facile process. The hydrolysis of the methoxide species to form methanol is also relatively facile from an energy perspective. The release of water from the active site has a moderate activation barrier unless N_2O is present in the gas phase.

Appendix

The basis set used for optimizing all structures reported in the main text, and also for evaluation of the corresponding energies, was the standard CRENBL effective core potential basis (see theoretical methods section for full details). This basis is quite large, essentially quadruple-ζ in the valence space. However, it does not contain polarization functions; that is, there are no f functions on the iron atom, and no d functions on C, O, Al, and Si. Since density functionals such as B3LYP are parametrized at the basis set limit, it is important to assess the sensitivity of the relative energetics that we have calculated to the addition of polarization functions.

To assess the significance of the incompleteness of the basis set used for this work, single-point energy calculations for the geometries reported above were carried out using the CRENBL basis augmented with polarization functions on all atoms. The standard polarization functions from the 6-311G** basis were used for H, C, O, Al, and Si. This is a reasonable choice since the CRENBL basis for H itself is 6-311G, and the size of the valence basis sets for C, O, Al, and Si is comparable to 6-311G also. For Fe, we employed a shell of f polarization functions of exponent 2.46, as recommended to augment the LANLDZ effective core potential basis.[37] The polarization functions were taken as pure rather than Cartesian functions.

The relative energies for all structures reported in Figures 2 through 5 are summarized in Table 2, with and without polarization functions. It can be seen that there are small shifts in all of the relative energies. The largest change is 9.2 kcal/mol, but the vast majority of changes are less than 5 kcal/mol.

The magnitude of these changes gives some indication of the uncertainty in our calculated results due to basis set incompleteness, although, of course, there may also be significant uncertainties due to limitations of the B3LYP functional itself. The most important results with respect to the predicted mechanism are the relative magnitudes of the barriers in Figures 2 and 5. It can be clearly seen from Table 2 that the addition of polarization functions in no way qualitatively affects the conclusion that the pathway of Figure 2 is strongly preferred based on its lower barrier.

Acknowledgment. This work was supported by a grant from BP International, Ltd. W.Z.L. expresses her thanks to G. Kong of Q-Chem, Inc., for helpful discussions related to the Q-Chem code.

References and Notes

(1) Anderson, J. R.; Tsai, P. *J. Chem. Soc., Chem. Comm*. **1987**, 1435.
(2) (a) Sobolev, V. I.; Dubkov, K. A.; Panna, O. V.; Panov, G. I. *Catal. Today* **1995**, *24*, 251. (b) Dubkov, K. A.; Sobolev, V. I.; Talsi, E. P.; Rodkin, M. A.; Watkins, N. H.; Shteinman, A. A.; Panov, G. I. *J. Mol. Catal. A.: Chem.* **1997**, *123*, 155.
(3) Wood, B. R.; Bell, A. T.; Reimer, J. A. private communication.
(4) Joyner, R.; Stockenhuber, M. *J. Phys. Chem. B* **1999**, *103*, 5963.
(5) Chen, H.-Y.; Sachtler, W. M. H. *Catal. Today* **1998**, *42*, 73.
(6) El-Malki, E.-M.; van Santen, R. A.; Sachtler, W. M. H. *J. Phys. Chem. B* **1999**, *103*, 4611.
(7) Marturano, P.; Drozdova, L.; Kogelbauer, A.; Prins, R. *J. Catal.* **2000**, *192*, 236.
(8) Marturano, P.; Drozdova, L.; Pirngruber, G.; Kogelbauer, A.; Prins, P. *Phys. Chem. Chem. Phys.* **2001**, *3*, 5585.
(9) Battiston, A. A.; Bitter, J. H.; Koningsberger, D. C. *Catal. Lett.* **2000**, *66*, 75.
(10) Jia, J.; Sun, Q.; Wen, B.; Chen, L. X.; Sachtler, W. H. M. *Catal. Lett.* **2002**, *82*, 7.
(11) Lobree, L. J.; Hwang, I.-C.; Reimer, J. A.; Bell, A. T. *J. Catal.* **1999**, *186*, 242.
(12) Wood, B. R.; Reimer, J. A.; Bell, A. T. *J. Catal.* **2002**, *209*, 151.
(13) Kucherov, A. V.; Shelef, M. *J. Catal*. **2000**, *195*, 106.
(14) Battison, A. A.; Bitter, J. H.; deGroot, F. M. F.; Overweg, A. R.; Stephan, O.; van Bokhaven, J. A.; Kooyman, P. J.; van der Spek; Vankó, G.; Koningsberger, D. C. *J. Catal*. **2003**, *213*, 251.
(15) Yoshizawa, K. *J. Inorg. Biochem*. **2000**, *78*, 23.
(16) Yoshizawa, K.; Shiota, Y.; Yumura, T.; Yamabe, T. *J. Phys. Chem. B* **2000**, *104*, 734.
(17) Yakovlev, A. L.; Zhidomirov, G. M.; van Santen, R. A. *J. Phys. Chem. B* **2001**, *105*, 12297.
(18) Ryder, J.; Chakraborty, A. K.; Bell, A. T. *J. Phys. Chem. B* **2002**, *106*, 7059.
(19) Ryder, J.; Charaborty, A. K.; Bell, A. T. *J. Catal.*, **2003**, *220*, 84.
(20) Choi, S. H.; Wood, B.; Ryder, J.; Bell, A. T. *J. Phys. Chem. B* **2003**, *107*, 11843.
(21) Andrews, L.; Chertihin, G. V.; Ricca, A.; Bauschlicher, C. W., Jr. *J. Am. Chem. Soc.* **1996**, *118*, 467.
(22) Garcia-Sosa, A. T.; Castro M. *Int. J. Quantum Chem.* **2000**, *80*, 307.
(23) Schröder, D.; Fiedler, A.; Schwarz, J.; Schwarz, H. *Inorg. Chem.* **1994**, *33*, 5094.
(24) Becke, A. D. *J. Chem. Phys*. **1993**, 98, 1372.
(25) Stephens, P. J.; Devlin, F. J.; Chabalowski, C. F.; Frisch, M. J. *J. Phys. Chem.* **1994**, *98*, 11623.
(26) (a) Pacios, L. F.; Christiansen, P. A. *J. Chem. Phys*. **1985**, 82, 2664. (b) Hurley, M. M.; Pacios, L. F.; Christiansen, P. A.; Ross, R. B.; Ermler, W. C. *J. Chem. Phys*. **1986**, 84, 6840. (c) LaJohn, T.; Christiansen, P. A.; Ross, R. B.; Ermler, W. C. *J. Chem. Phys*. **1987**, 87, 2812.
(27) (a) Walt, W. R. and Hay, P. J. *J. Chem. Phys*. **1985,** 82, 285. (b) Hay, P. J.; Walt, W. R. *J. Chem. Phys*. **1985**, 82, 299.
(28) Dolg, M.; Wedig, U.; Stoll, H.; Preuss, H. *J. Chem. Phys*. **1987**, 86, 866.
(29) Kong, J.; White, C. A.; Krylov, A. I.; Sherrill, C. D.; Adamson, R. D.; Furlani, T. R.; Lee, M. S.; Lee, A. M. Gwaltney, S. R.; Adams, T. R. Ochsenfeld, C.; Gilbert, A. T. B.; Kedziora, G. S.; Rassolov, V. A.; Maurice, D. R.; Nair, N.; Shao, Y.; Besley, N. A.; Maslen, P. E.; Dombroski, J. P.; Daschel, H.; Zhang, W.; Korambath, P. P.; Baker, J.; Byrd, E. F. C.; Voorhis, T. Van; Oumi, M.; Hirata, S.; Hsu, C. P.; Ishikawa, N.; Florian, J.; Warshel, A.; Johnson, B. G.; Gill, P. M. W.; Head Gordon, M.; Pople, J. A. *J. Comput. Chem.* **2000**, *21*, 1532.
(30) Jones, R. D.; Summerville, D. A.; Basolo, F. *Chem. Rev.* **1979**, *79*, 139.
(31) (a) Que, L., Jr. In *Bioinorganic Catalysis*, 2nd ed.; Redijk, J., Bouwmann., Eds.; Marcel Dekker: New York, 1999; pp 269−322. (b) Ingold, K. U.; MacFaul, P. A. In *Biomimetic Oxidation Catalyzed by Transition Metal Complexes*; Meunier, B., Ed.; Imperial College Press: London, 2000; pp 45−90.
(32) Schröder, D.; Schwarz, H. *Angew. Chem., Int. Ed. Engl*. **1990**, *29*, 1433.
(33) Schröder, D.; Fiedler, A.; Hrusàk, J.; Schwarz, H. *J. Am. Chem. Soc.* **1992**, *114*, 1215.
(34) Schröder, D.; Schwarz, H.; Clemmer, D. E.; Chen, Y. M.; Armentrout, P. B.; Baranov, V. I.; Böhme, D. K. *Int. J. Mass Spectrum. Ion Processes* **1997**, *161*, 175.
(35) Schröder, D.; Schwarz, H. *Angew. Chem., Int. Ed. Engl*. **1995**, *34*, 1973.
(36) (a) Shaik, S.; Danovich, D.; Fiedler, A.; Schröder, D.; Schwarz, H. *Helv. Chim. Acta* **1995**, *78*, 1393. (b) Shaik, S.; Filatov, M.; Schröder, D.; Schwarz, H. *Chem. Eur. J.* **1998**, *4*, 193.
(37) Ehlers, A. W.; Bohme, M.; Dapprich, S.; Gobbi, A.; Hollwarth, A.; Jonas, V.; Kohler, K. F.; Stegmann, R.; Veldkamp, A.; Frenking, G. *Chem. Phys. Lett.* **1993**, *208*, 111.